Nonlinear Dyn (2007) 47:181–192
DOI 10.1007/s11071-006-9064-6

ORIGINAL ARTICLE

Primary resonance excitation of electrically actuated clamped circular plates

Gregory W. Vogl · Ali H. Nayfeh

Received: 19 October 2005 / Accepted: 17 December 2006 / Published online: 28 November 2006

Abstract We investigate the response of an electrically actuated clamped circular plate to a primary resonance excitation of its first axisymmetric mode using an analytical reduced-order model (macromodel). We discuss the influence of the number of modes retained in the discretization on the predicted solutions. The reduced-order model, which is a system of coupled nonlinear ordinary-differential equations, accounts for general residual stress and strain hardening and allows for general material and geometric design variables. Our reduced-order model is robust up to the pull-in instability and is general enough to be an effective design tool for capacitive micromachined ultrasonic transducers.

Keywords CMUT · Electrostatic actuation · Macromodel · Pull-in · Reduced-order model

1. Introduction

Circular microplates are commonly electrically actuated in capacitive micromachined ultrasonic transducers (CMUTs) in both air [1–9] and liquids [4, 10–12]. The circular microplate is typically composed of a single silicon crystal or silicon nitride and is suspended above a heavily doped silicon bulk material. When a bias voltage is applied between a deposited conductive material (the top electrode) on the microplate and the bulk base (the bottom electrode), the attractive electrostatic forces cause the microplate to deflect downward. If a small alternating voltage is added to the bias voltage, then relatively large displacements can be created when the frequency is near resonance, causing significant sound generation [2]. The CMUT converts electrical energy into mechanical energy and vice versa [9], and a good design requires a large displacement from the bias voltage for efficient energy coupling between the circular microplate and the air [1]. The microplate can also be deflected by ambient pressure if the cavity beneath the microplate is vacuum sealed [8], which is necessary for immersion applications. Optimum energy coupling is achieved when the plate is near the structural instability known as 'pull-in' [9], where the largest stable plate deflection occurs.

Many resonance applications demand better understanding of CMUT behavior. Many researchers use FEM simulations [6 8, 9, 13–15], analytical plate or membrane models [1–3, 5, 10, 16, 17], or lumped-element models [9, 14] to analyze resonating circular microstructures. These approaches have their respective flaws. Most FEM simulations are computationally inefficient or breakdown near pull-in of electrostatically actuated structures, and membrane models ignore plate bending, which is needed for bending-dominated microstructures. Furthermore,

G. W. Vogl · A. H. Nayfeh (✉)
Department of Engineering Science and Mechanics, MC 0219, Virginia Polytechnic Institute and State University, Blacksburg, VA 24061, USA
e-mail: anayfeh@vt.edu

analytical plate or plate-membrane models usually ignore nonlinearities [18], such as those created by large plate deflections, so linear theories may produce inaccurate results. Then, a geometrically nonlinear elastic analysis needs to be utilized [19].

We investigate the response of a clamped circular plate to a primary resonance excitation of its first mode through reduced-order modeling, which is atypical for electrostatically actuated circular plates. We use the analytical reduced-order model (macromodel) for an electrostatically actuated clamped circular plate that was developed in an earlier paper [20]. The reduced-order model, which is a system of N coupled nonlinear ordinary-differential equations, accounts for general residual stress and allows for general material and geometric design variables. The reduced-order model uses a full plate model and is robust up to the pull-in instability. Furthermore, large deformations are allowed because the first geometric nonlinearity of the von Kármán type is included in the model [21]. Consequently, the reduced-order model captures the complex multi-energy-domain physics in a relatively simple and compact model and is general enough to be an effective design tool.

2. System equations

A schematic of a circular plate under electrostatic actuation is shown in Fig. 1. The plate has a radius R, thickness h, and is fully clamped above a parallel electrode with an effective electrode separation distance d. When a voltage $\hat{v}(\hat{t})$ is applied between the plate and electrode at time $\hat{t}$, the plate will deflect towards the fixed electrode. For an isotropic plate with a uniform residual biaxial plane stress $\hat{\tau}$, the transverse deflection $\hat{w}$ is axisymmetric when the plate is electrically actuated from rest. Furthermore, because of the fully clamped boundary condition, the residual stress does not cause the initial deflections that occur for other boundary conditions [6].

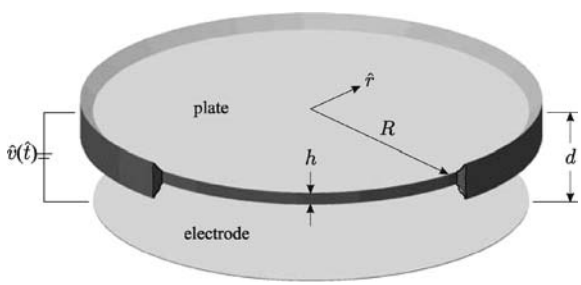

Fig. 1 A schematic of electric actuation of a clamped circular plate

An approximate analytical model [21]

$$w(r,t) = \sum_{m=1}^{N} \eta_m(t)\phi_m(r) \tag{1}$$

has been created for the nondimensional axisymmetric deflection $w(r,t)$ of a clamped circular plate, where t and r are the nondimensional temporal and spatial variables, respectively. The shape functions $\phi_m(r)$ seen in Equation (1) are the first N axisymmetric modes of the linear undamped case with zero residual stress and no electrostatic forcing, and $\eta_m(t)$ is the generalized coordinate associated with the mth shape function. All $\eta_m(t)$ can be determined by solving the following system of N coupled nonlinear ordinary-differential equations in matrix form:

$$M(\boldsymbol{\eta})\ddot{\boldsymbol{\eta}} + 2cM(\boldsymbol{\eta})\dot{\boldsymbol{\eta}} + N(\boldsymbol{\eta})\boldsymbol{\eta} = \boldsymbol{P}(\boldsymbol{\eta}) + v^2(t)\boldsymbol{L}, \tag{2}$$

where the matrices $M(\boldsymbol{\eta})$ and $N(\boldsymbol{\eta})$ and the vector $\boldsymbol{P}(\boldsymbol{\eta})$ are nonlinear functions of $\boldsymbol{\eta}(t) = \{\eta_1(t),\ \eta_2(t), \ldots,\ \eta_N(t)\}$, $\boldsymbol{L}$ is a constant vector, c is a nondimensional damping parameter, and $v(t)$ is the nondimensional potential difference between the ground and the electrode on the plate. The matrices M and N and the vectors $\boldsymbol{P}$ and $\boldsymbol{L}$ are defined in Appendix A.

The $N \times N$ matrices M and N and N-length vector $\boldsymbol{P}$ are functions of a nondimensional residual stress τ, Poisson's ratio ν, the number of modes N, an axisymmetric downward pressure difference $F(r,t)$ on the plate, and a nondimensional parameter β defined as

$$\beta = 12\left(\frac{d}{h}\right)^2(1-\nu^2).$$

Once all $\eta_m(t)$ are determined by solving the nonlinear matrix equation (2), the plate deflection $w(r,t)$ is given approximately by Equation (1).

3. Primary resonance of the first mode

We investigate the response of a clamped circular plate to a primary resonance excitation of its first mode. Hence, we let the nondimensional voltage $v(t)$ be

$$v(t) = \chi_0 + \chi_3 \cos(\omega_f t), \tag{3a}$$

where the forcing frequency ω_f is defined as

$$\omega_f = \omega_1 + \sigma, \tag{3b}$$

and the detuning parameter σ represents how far the forcing frequency is from the first natural frequency ω_1 of the plate around its deformed equilibrium state. Physically, the parameters χ_0 and χ_3 are associated with the DC and AC voltage components, respectively. The nondimensional DC voltage χ_0 causes the plate to deform towards the fixed electrode, and the first frequency ω_1 is then determined for the deflected equilibrium.

Following the method of multiple scales (MMS) [22, 23], we seek a third-order approximate solution of Equation (2) in the form

$$\begin{aligned}\boldsymbol{\eta}(t;\epsilon) = \boldsymbol{\eta}_0 + \epsilon\boldsymbol{\eta}_1(T_0,\ T_1,\ T_2) + \epsilon^2\boldsymbol{\eta}_2(T_0,\ T_1,\ T_2)\\ + \epsilon^3\boldsymbol{\eta}_3(T_0,\ T_1,\ T_2) + O(\epsilon^4)\end{aligned} \tag{4}$$

where $T_n = \epsilon^n t$ and ϵ is a small bookkeeping parameter. In order that the nonlinearity balance the effects of the damping and forcing, we introduce the following scaled variables *a priori*:

$$c \to \epsilon^2 c, \quad \chi_3 \to \epsilon^3\chi_3, \quad \text{and} \quad \sigma \to \epsilon^2\sigma, \tag{5}$$

and rewrite Equation (2) as

$$M(\boldsymbol{\eta})\ddot{\boldsymbol{\eta}} + 2\epsilon^2 c M(\boldsymbol{\eta})\dot{\boldsymbol{\eta}} + N(\boldsymbol{\eta})\boldsymbol{\eta} = P(\boldsymbol{\eta}) + v^2(t)\boldsymbol{L}. \tag{6}$$

Moreover, we express the cosine function in Equation (3a) in terms of exponentials, apply the new scaling for the detuning parameter σ, and then use the time scales T_n to obtain

$$v(t) = \chi_0 + \frac{1}{2}\epsilon^3\chi_3(\mathrm{e}^{\mathrm{i}\sigma T_2}\mathrm{e}^{\mathrm{i}\omega_1 T_0} + \mathrm{e}^{-\mathrm{i}\sigma T_2}\mathrm{e}^{-\mathrm{i}\omega_1 T_0}). \tag{7}$$

We substitute Equations (4) and (7) into Equation (6), expand all matrices and vectors that are functions of $\boldsymbol{\eta}$ in powers of ϵ, collect terms of orders of ϵ up to $O(\epsilon^3)$, and obtain the following equations:

Order(1)

$$N_0\,\boldsymbol{\eta}_0 - \boldsymbol{P}_0 - \chi_0^2\boldsymbol{L} = \boldsymbol{0} \tag{8}$$

Order(ϵ)

$$M_0\,D_0^2\boldsymbol{\eta}_1 + N_0\,\boldsymbol{\eta}_1 + N_1(\boldsymbol{\eta}_1)\,\boldsymbol{\eta}_0 - P_1\,\boldsymbol{\eta}_1 = \boldsymbol{0} \tag{9}$$

Order(ϵ^2)

$$\begin{aligned}&M_0\,D_0^2\boldsymbol{\eta}_2 + N_0\,\boldsymbol{\eta}_2 + N_1(\boldsymbol{\eta}_2)\,\boldsymbol{\eta}_0 - P_1\,\boldsymbol{\eta}_2\\ &\quad= -2M_0\,D_0D_1\boldsymbol{\eta}_1 - M_1(\boldsymbol{\eta}_1)\,D_0^2\boldsymbol{\eta}_1\\ &\quad -N_1(\boldsymbol{\eta}_1)\,\boldsymbol{\eta}_1 - N_2(\boldsymbol{\eta}_1,\boldsymbol{\eta}_1)\,\boldsymbol{\eta}_0 + \boldsymbol{P}_2(\boldsymbol{\eta}_1,\boldsymbol{\eta}_1)\end{aligned} \tag{10}$$

Order(ϵ^3)

$$\begin{aligned}&M_0\,D_0^2\boldsymbol{\eta}_3 + N_0\,\boldsymbol{\eta}_3 + N_1(\boldsymbol{\eta}_3)\,\boldsymbol{\eta}_0 - P_1\,\boldsymbol{\eta}_3\\ &\quad= -2cM_0\,D_0\boldsymbol{\eta}_1 - 2M_0\,D_0D_1\boldsymbol{\eta}_2\\ &\quad -M_0\,D_1^2\boldsymbol{\eta}_1 - 2M_0\,D_0D_2\boldsymbol{\eta}_1 - M_1(\boldsymbol{\eta}_1)\,D_0^2\boldsymbol{\eta}_2\\ &\quad -2M_1(\boldsymbol{\eta}_1)\,D_0D_1\boldsymbol{\eta}_1\\ &\quad -M_1(\boldsymbol{\eta}_2)\,D_0^2\boldsymbol{\eta}_1 - M_2(\boldsymbol{\eta}_1,\boldsymbol{\eta}_1)\,D_0^2\boldsymbol{\eta}_1\\ &\quad -N_1(\boldsymbol{\eta}_1)\,\boldsymbol{\eta}_2 - N_1(\boldsymbol{\eta}_2)\,\boldsymbol{\eta}_1\\ &\quad -N_2(\boldsymbol{\eta}_1,\boldsymbol{\eta}_1)\,\boldsymbol{\eta}_1 - 2N_2(\boldsymbol{\eta}_1,\boldsymbol{\eta}_2)\,\boldsymbol{\eta}_0\\ &\quad -N_3(\boldsymbol{\eta}_1,\boldsymbol{\eta}_1,\boldsymbol{\eta}_1)\,\boldsymbol{\eta}_0 + 2\boldsymbol{P}_2(\boldsymbol{\eta}_1,\boldsymbol{\eta}_2)\\ &\quad +\boldsymbol{P}_3(\boldsymbol{\eta}_1,\boldsymbol{\eta}_1,\boldsymbol{\eta}_1)\\ &\quad +\chi_0\chi_3\left(\mathrm{e}^{\mathrm{i}\sigma T_2}\mathrm{e}^{\mathrm{i}\omega_1 T_0} + \mathrm{e}^{-\mathrm{i}\sigma T_2}\mathrm{e}^{-\mathrm{i}\omega_1 T_0}\right)\boldsymbol{L}\end{aligned} \tag{11}$$

where $D_i = \frac{\partial}{\partial T_i}$, $\boldsymbol{0}$ is the zero vector of length N,

$$M_0 = M(\boldsymbol{\eta}_0), \quad N_0 = N(\boldsymbol{\eta}_0), \tag{12a}$$

$$\boldsymbol{P}_0 = \boldsymbol{P}(\boldsymbol{\eta}_0), \tag{12b}$$

$$M_1(\boldsymbol{x}) = \left[\frac{\partial M}{\partial \eta_i}\boldsymbol{x}_i\right], \quad N_1(\boldsymbol{x}) = \left[\frac{\partial N}{\partial \eta_i}\boldsymbol{x}_i\right], \tag{12c}$$

$$P_1 = [P_{1ij}] = \left[\frac{\partial \boldsymbol{P}_i}{\partial \eta_j}\right], \tag{12d}$$

$$M_2(\boldsymbol{x},\boldsymbol{y}) = \left[\frac{1}{2}\frac{\partial^2 M}{\partial\eta_i\partial\eta_j}\boldsymbol{x}_i\boldsymbol{y}_j\right], \tag{12e}$$

$$N_2(\boldsymbol{x},\boldsymbol{y}) = \left[\frac{1}{2}\frac{\partial^2 N}{\partial\eta_i\partial\eta_j}\boldsymbol{x}_i\boldsymbol{y}_j\right], \tag{12f}$$

$$\boldsymbol{P}_2(\boldsymbol{x},\boldsymbol{y}) = \{P_{2k}(\boldsymbol{x},\boldsymbol{y})\} = \left\{\frac{1}{2}\frac{\partial^2 \boldsymbol{P}_k}{\partial\eta_i\partial\eta_j}\boldsymbol{x}_i\boldsymbol{y}_j\right\}, \tag{12g}$$

$$N_3(\boldsymbol{x},\boldsymbol{y},\boldsymbol{z}) = \left[\frac{1}{6}\frac{\partial^3 N}{\partial\eta_i\partial\eta_j\partial\eta_k}\boldsymbol{x}_i\boldsymbol{y}_j\boldsymbol{z}_k\right], \tag{12h}$$

and

$$\boldsymbol{P}_3(\boldsymbol{x},\boldsymbol{y},\boldsymbol{z}) = \{P_{3k}(\boldsymbol{x},\boldsymbol{y},\boldsymbol{z})\} = \left[\frac{1}{6}\frac{\partial^3 \boldsymbol{P}_k}{\partial\eta_i\partial\eta_j\partial\eta_k}\boldsymbol{x}_i\boldsymbol{y}_j\boldsymbol{z}_k\right]. \tag{12i}$$

Here, $\boldsymbol{v}_i$ is the ith component of a general vector $\boldsymbol{v}$, all derivatives are evaluated at $\boldsymbol{\eta} = \boldsymbol{\eta}_0$, and Einstein's summation convention is used.

Before solving Equations (8)–(11), we rearrange their left-hand sides and rewrite them as

Order(1)

$$N_0\,\boldsymbol{\eta}_0 - \boldsymbol{P}_0 - \chi_0^2\boldsymbol{L} = \boldsymbol{0} \tag{13}$$

Order(ϵ)

$$M_0\,D_0^2\boldsymbol{\eta}_1 + R_0\,\boldsymbol{\eta}_1 = \boldsymbol{0} \tag{14}$$

Order(ϵ^2)

$$\begin{aligned} M_0\,D_0^2\boldsymbol{\eta}_2 + R_0\,\boldsymbol{\eta}_2 &= -2M_0\,D_0D_1\boldsymbol{\eta}_1 \\ &\quad -M_1(\boldsymbol{\eta}_1)\,D_0^2\boldsymbol{\eta}_1 - N_1(\boldsymbol{\eta}_1)\,\boldsymbol{\eta}_1 \\ &\quad -N_2(\boldsymbol{\eta}_1,\boldsymbol{\eta}_1)\,\boldsymbol{\eta}_0 + \boldsymbol{P}_2(\boldsymbol{\eta}_1,\boldsymbol{\eta}_1) \end{aligned} \tag{15}$$

Order(ϵ^3)

$$\begin{aligned} M_0\,D_0^2\boldsymbol{\eta}_3 + R_0\,\boldsymbol{\eta}_3 &= -2cM_0\,D_0\boldsymbol{\eta}_1 \\ &\quad -2M_0\,D_0D_1\boldsymbol{\eta}_2 - M_0\,D_1^2\boldsymbol{\eta}_1 - 2M_0\,D_0D_2\boldsymbol{\eta}_1 \\ &\quad -M_1(\boldsymbol{\eta}_1)\,D_0^2\boldsymbol{\eta}_2 - 2M_1(\boldsymbol{\eta}_1)\,D_0D_1\boldsymbol{\eta}_1 \\ &\quad -M_1(\boldsymbol{\eta}_2)\,D_0^2\boldsymbol{\eta}_1 - M_2(\boldsymbol{\eta}_1,\boldsymbol{\eta}_1)\,D_0^2\boldsymbol{\eta}_1 \\ &\quad -N_1(\boldsymbol{\eta}_1)\,\boldsymbol{\eta}_2 - N_1(\boldsymbol{\eta}_2)\,\boldsymbol{\eta}_1 - N_2(\boldsymbol{\eta}_1,\boldsymbol{\eta}_1)\,\boldsymbol{\eta}_1 \\ &\quad -2N_2(\boldsymbol{\eta}_1,\boldsymbol{\eta}_2)\,\boldsymbol{\eta}_0 - N_3(\boldsymbol{\eta}_1,\boldsymbol{\eta}_1,\boldsymbol{\eta}_1)\,\boldsymbol{\eta}_0 \\ &\quad +2\boldsymbol{P}_2(\boldsymbol{\eta}_1,\boldsymbol{\eta}_2) + \boldsymbol{P}_3(\boldsymbol{\eta}_1,\boldsymbol{\eta}_1,\boldsymbol{\eta}_1) \\ &\quad +\chi_0\chi_3\left(\mathrm{e}^{\mathrm{i}\sigma T_2}\mathrm{e}^{\mathrm{i}\omega_1 T_0} + \mathrm{e}^{-\mathrm{i}\sigma T_2}\mathrm{e}^{-\mathrm{i}\omega_1 T_0}\right)\boldsymbol{L} \end{aligned} \tag{16}$$

where $R_0 = N_0 - P_1 + Q_0$ and

$$Q_0 = \left[\left\{\frac{\partial N}{\partial\eta_1}\boldsymbol{\eta}_0\right\}\left\{\frac{\partial N}{\partial\eta_2}\boldsymbol{\eta}_0\right\}\ \cdots\ \left\{\frac{\partial N}{\partial\eta_N}\boldsymbol{\eta}_0\right\}\right]\Bigg|_{\boldsymbol{\eta}_0}. \tag{17}$$

We now solve Equations (13)–(16) sequentially, starting with Equation (13). The equations are solved symbolically here and numerical solutions are generated afterwards.

Order(1)

If χ_0 is less than its pull-in value χ_0^{pi}, the nondimensional DC voltage χ_0 causes the plate to deform towards the fixed electrode and reach a new static equilibrium state. We solve the nonlinear matrix equation (13) numerically.

Order(ϵ)

If M_0 is nonsingular, then Equation (14) can be rearranged as

$$D_0^2\boldsymbol{\eta}_1 + S_0\,\boldsymbol{\eta}_1 = \boldsymbol{0}, \tag{18}$$

where $S_0 = M_0^{-1}R_0$ is a known matrix function of $\boldsymbol{\eta}_0$. Assuming that $\boldsymbol{\eta}_1 = A(T_1,T_2)\mathrm{e}^{\mathrm{i}\omega T_0}\boldsymbol{p}$ is a solution of Equation (18), we obtain the eigenvalue problem

$$S_0\,\boldsymbol{p} = \omega^2\boldsymbol{p}. \tag{19}$$

We consider the case in which Equation (19) has N unique real eigenvalues $\omega_1^2, \omega_2^2, \ldots, \omega_N^2$ and associated real eigenvectors $\boldsymbol{p}_1, \boldsymbol{p}_2, \ldots, \boldsymbol{p}_N$, which represent the undamped natural frequencies and mode shapes around the deflected configuration, respectively. Consequently, the general solution of Equation (18) can be expressed as

$$\boldsymbol{\eta}_1 = \sum_{k=1}^{N}\left(A_k(T_1,T_2)\mathrm{e}^{\mathrm{i}\omega_k T_0}\boldsymbol{p}_k + \bar{A}_k(T_1,T_2)\mathrm{e}^{-\mathrm{i}\omega_k T_0}\boldsymbol{p}_k\right), \tag{20}$$

where A_k is a complex measure of the vibration amplitude and phase of the kth mode, and the overbar denotes the complex conjugate of an expression. We

consider the case in which the first mode is excited with a primary resonance and not involved in an internal resonance with any other mode. Because in the presence of damping all of the modes that are not directly or indirectly excited decay with time [24, 25], the long-time response of Equation (18) can be expressed as

$$\boldsymbol{\eta}_1 = A(T_1, T_2)\mathrm{e}^{\mathrm{i}\omega_1 T_0}\boldsymbol{p}_1 + \bar{A}(T_1, T_2)\mathrm{e}^{-\mathrm{i}\omega_1 T_0}\boldsymbol{p}_1. \tag{21}$$

Order(ϵ^2)

Substituting for $\boldsymbol{\eta}_0$ and $\boldsymbol{\eta}_1$ in Equation (15), we obtain

$$\begin{aligned} M_0 D_0^2\boldsymbol{\eta}_2 + R_0\boldsymbol{\eta}_2 = &-2\mathrm{i}\omega_1 D_1 A\,\mathrm{e}^{\mathrm{i}\omega_1 T_0}M_0\boldsymbol{p}_1 \\ &+2\mathrm{i}\omega_1 D_1\bar{A}\,\mathrm{e}^{-\mathrm{i}\omega_1 T_0}M_0\boldsymbol{p}_1 \\ &+\omega_1^2 A^2\mathrm{e}^{2\mathrm{i}\omega_1 T_0}M_1(\boldsymbol{p}_1)\boldsymbol{p}_1+\omega_1^2\bar{A}^2\mathrm{e}^{-2\mathrm{i}\omega_1 T_0}M_1(\boldsymbol{p}_1)\boldsymbol{p}_1 \\ &+2\omega_1^2 A\bar{A}M_1(\boldsymbol{p}_1)\boldsymbol{p}_1 \\ &-A^2\mathrm{e}^{2\mathrm{i}\omega_1 T_0}N_1(\boldsymbol{p}_1)\boldsymbol{p}_1 - \bar{A}^2\mathrm{e}^{-2\mathrm{i}\omega_1 T_0}N_1(\boldsymbol{p}_1)\boldsymbol{p}_1 \\ &-2A\bar{A}N_1(\boldsymbol{p}_1)\boldsymbol{p}_1 \\ &-A^2\mathrm{e}^{2\mathrm{i}\omega_1 T_0}N_2(\boldsymbol{p}_1,\boldsymbol{p}_1)\boldsymbol{\eta}_0 \\ &-\bar{A}^2\mathrm{e}^{-2\mathrm{i}\omega_1 T_0}N_2(\boldsymbol{p}_1,\boldsymbol{p}_1)\boldsymbol{\eta}_0 \\ &-2A\bar{A}N_2(\boldsymbol{p}_1,\boldsymbol{p}_1)\boldsymbol{\eta}_0 \\ &+A^2\mathrm{e}^{2\mathrm{i}\omega_1 T_0}\boldsymbol{P}_2(\boldsymbol{p}_1,\boldsymbol{p}_1) + \bar{A}^2\mathrm{e}^{-2\mathrm{i}\omega_1 T_0}\boldsymbol{P}_2(\boldsymbol{p}_1,\boldsymbol{p}_1) \\ &+2A\bar{A}\boldsymbol{P}_2(\boldsymbol{p}_1,\boldsymbol{p}_1). \end{aligned} \tag{22}$$

We want to solve for $\boldsymbol{\eta}_2$, but we need to eliminate secular solutions to ensure uniformity of the expansion. In the absence of internal resonances, the only terms that produce secular terms are the terms on the right-hand side proportional to $\mathrm{e}^{\mathrm{i}\omega_1 T_0}$ or $\mathrm{e}^{-\mathrm{i}\omega_1 T_0}$. A uniform solution for $\boldsymbol{\eta}_2$ exists only if the terms that produce secular terms are orthogonal to every solution $\boldsymbol{u}_1$ of the adjoint homogeneous problem associated with ω_1, given as

$$\omega_1^2 M_0^T\boldsymbol{u}_1 = R_0^T\boldsymbol{u}_1. \tag{23}$$

Impozing the solvability condition on Equation (22) demands that

$$D_1 A = 0 \quad\Longrightarrow\quad A(T_1, T_2) = A(T_2). \tag{24}$$

The general solution of Equation (22) consists of a homogeneous component and a particular component. We "lump" the homogeneous component for $\boldsymbol{\eta}_2$ with the homogeneous solution for $\boldsymbol{\eta}_1$, since they are of the same form, leaving us with the following particular solution for $\boldsymbol{\eta}_2$:

$$\boldsymbol{\eta}_2 = A^2\mathrm{e}^{2\mathrm{i}\omega_1 T_0}\boldsymbol{z}_1 + \bar{A}^2\mathrm{e}^{-2\mathrm{i}\omega_1 T_0}\boldsymbol{z}_1 + A\bar{A}\boldsymbol{z}_2, \tag{25}$$

where

$$\begin{aligned} \boldsymbol{z}_1 = &\left[R_0 - 4\omega_1^2 M_0\right]^{-1}\left\{\omega_1^2 M_1(\boldsymbol{p}_1)\boldsymbol{p}_1\right. \\ &\left.- N_1(\boldsymbol{p}_1)\boldsymbol{p}_1 - N_2(\boldsymbol{p}_1,\boldsymbol{p}_1)\boldsymbol{\eta}_0 + \boldsymbol{P}_2(\boldsymbol{p}_1,\boldsymbol{p}_1)\right\}, \end{aligned} \tag{26a}$$

and

$$\begin{aligned} \boldsymbol{z}_2 = &\,2R_0^{-1}\left\{\omega_1^2 M_1(\boldsymbol{p}_1)\boldsymbol{p}_1\right. \\ &\left.- N_1(\boldsymbol{p}_1)\boldsymbol{p}_1 - N_2(\boldsymbol{p}_1,\boldsymbol{p}_1)\boldsymbol{\eta}_0 + \boldsymbol{P}_2(\boldsymbol{p}_1,\boldsymbol{p}_1)\right\}. \end{aligned} \tag{26b}$$

Order(ϵ^3)

As with $\boldsymbol{\eta}_2$, a uniform solution for $\boldsymbol{\eta}_3$ exists only if the terms that produce secular terms at $O(\epsilon^3)$ are orthogonal to $\boldsymbol{u}_1$. Substituting for $\boldsymbol{\eta}_0$, $\boldsymbol{\eta}_1$, and $\boldsymbol{\eta}_2$ in Equation (16), using Equation (24), collecting terms proportional to $\mathrm{e}^{\mathrm{i}\omega_1 T_0}$, and making the vector sum be orthogonal to $\boldsymbol{u}_1$, we obtain the solvability condition

$$\begin{aligned} &(\boldsymbol{u}_1\cdot\boldsymbol{v}_1)A' + c\,(\boldsymbol{u}_1\cdot\boldsymbol{v}_1)A \\ &\quad+(\boldsymbol{u}_1\cdot\boldsymbol{v}_2)A^2\bar{A} + (\chi_0\boldsymbol{u}_1\cdot\boldsymbol{L})\,\mathrm{e}^{\mathrm{i}\sigma T_2}\chi_3 = 0, \end{aligned} \tag{27}$$

where

$$\boldsymbol{v}_1 = -2\mathrm{i}\omega_1 M_0\boldsymbol{p}_1, \tag{28a}$$

$$\begin{aligned} \boldsymbol{v}_2 = &\,\omega_1^2 M_1(\boldsymbol{z}_1)\boldsymbol{p}_1 + \omega_1^2 M_1(\boldsymbol{z}_2)\boldsymbol{p}_1 \\ &+ 3\omega_1^2 M_2(\boldsymbol{p}_1,\boldsymbol{p}_1)\boldsymbol{p}_1 - N_1(\boldsymbol{z}_1)\boldsymbol{p}_1 \\ &- N_1(\boldsymbol{z}_2)\boldsymbol{p}_1 - 3N_2(\boldsymbol{p}_1,\boldsymbol{p}_1)\boldsymbol{p}_1 \\ &+ 4\omega_1^2 M_1(\boldsymbol{p}_1)\boldsymbol{z}_1 - N_1(\boldsymbol{p}_1)\boldsymbol{z}_1 - N_1(\boldsymbol{p}_1)\boldsymbol{z}_2 \\ &- 2N_2(\boldsymbol{p}_1,\boldsymbol{z}_1)\boldsymbol{\eta}_0 - 2N_2(\boldsymbol{p}_1,\boldsymbol{z}_2)\boldsymbol{\eta}_0 \\ &- 3N_3(\boldsymbol{p}_1,\boldsymbol{p}_1,\boldsymbol{p}_1)\boldsymbol{\eta}_0 + 2\boldsymbol{P}_2(\boldsymbol{p}_1,\boldsymbol{z}_1) \\ &+ 2\boldsymbol{P}_2(\boldsymbol{p}_1,\boldsymbol{z}_2) + 3\boldsymbol{P}_3(\boldsymbol{p}_1,\boldsymbol{p}_1,\boldsymbol{p}_1), \end{aligned} \tag{28b}$$

and the prime denotes differentiation with respect to T_2. Now, because the eigenvector $\boldsymbol{u}_1$ is known to within an arbitrary constant, we normalize $\boldsymbol{u}_1$ such that

$$\boldsymbol{u}_1 \cdot \boldsymbol{v}_1 = 1$$

and reduce Equation (27) to

$$A' + cA - 4\mathrm{i}\alpha_1 A^2 \bar{A} + \frac{1}{2}\mathrm{i}\alpha_2 \mathrm{e}^{\mathrm{i}\sigma T_2}\chi_3 = 0, \tag{29}$$

where α_1 and α_2 are real and defined as

$$\alpha_1 = \frac{1}{4}\mathrm{i}\boldsymbol{u}_1 \cdot \boldsymbol{v}_2 \tag{30a}$$

and

$$\alpha_2 = -2\mathrm{i}\chi_0 \boldsymbol{u}_1 \cdot \boldsymbol{L}. \tag{30b}$$

4. Modulation equations

To solve Equation (29), we first transform it into two coupled real equations using the transformation

$$A(T_2) = \frac{1}{2}a(T_2)\mathrm{e}^{\mathrm{i}\theta(T_2)}, \tag{31}$$

where $a(T_2)$ and $\theta(T_2)$ are real functions. Substituting Equations (21), (25), and (31) into Equation (4), we have

$$\begin{aligned}\boldsymbol{\eta}(t;\epsilon) = {} & \boldsymbol{\eta}_0 + \epsilon\, a(T_2)\cos(\omega_1 T_0 + \theta(T_2))\,\boldsymbol{p}_1 \\ & + \frac{1}{2}\epsilon^2 a^2(T_2)\Big[\cos(2\omega_1 T_0 + 2\theta(T_2))\,\boldsymbol{z}_1 \\ & + \frac{1}{2}\boldsymbol{z}_2\Big] + O(\epsilon^3).\end{aligned} \tag{32}$$

Because ϵ is a bookkeeping parameter, we absorb ϵ into a by letting $\epsilon a \rightarrow a$, such that a is now small. In other words, we let ϵ be equal to one, with the understanding that a is small, and rewrite Equation (32) as

$$\begin{aligned}\boldsymbol{\eta}(t) = {} & \boldsymbol{\eta}_0 + a(t)\cos(\omega_{\mathrm{f}} t + \gamma(t))\,\boldsymbol{p}_1 \\ & + \frac{1}{2}a^2(t)\Big[\cos(2\omega_{\mathrm{f}} t + 2\gamma(t))\,\boldsymbol{z}_1 + \frac{1}{2}\boldsymbol{z}_2\Big] \\ & + O(a^3),\end{aligned} \tag{33}$$

where $\gamma(t) = \theta(t) - \sigma t$. If a is sufficiently small and $\|\boldsymbol{p}_1\| = 1$, then the functions $a(t)$ and $\theta(t)$ represent the amplitude and phase of the response of the plate, respectively.

Substituting Equation (31) into Equation (29) and separating real and imaginary parts yields the following autonomous set of modulation equations:

$$\dot{a} = -ca - \alpha_2\chi_3 \sin(\gamma) \tag{34}$$

and

$$\dot{\gamma} = \alpha_1 a^2 - \sigma - \frac{\alpha_2\chi_3\cos(\gamma)}{a}. \tag{35}$$

5. Frequency-response (F-R) equation

The equations governing the equilibrium values a_{eq} and γ_{eq} of Equations (34) and (35) are found by setting $\dot{a} = 0$ and $\dot{\gamma} = 0$. They are given by

$$0 = -ca - \alpha_2\chi_3 \sin(\gamma) \tag{36}$$

and

$$0 = \alpha_1 a^2 - \sigma - \frac{\alpha_2\chi_3\cos(\gamma)}{a}. \tag{37}$$

Eliminating γ from Equations (36) and (37) yields the frequency-response (F-R) equation

$$a_{\mathrm{eq}}^2\left\{c^2 + (\sigma - \alpha_1 a_{\mathrm{eq}}^2)^2\right\} = \alpha_2^2\chi_3^2. \tag{38}$$

A point on the frequency-response curve is asymptotically stable if the eigenvalues λ_1 and λ_2 of the Jacobian matrix of the right-hand sides of Equations (34) and (35) at that point are in the left-half of the complex plane.

6. Nonlinear resonance

The nonlinear resonance frequency occurs at the peak of the F-R curve; that is, the maximum value a_{nr} in the $\sigma - a_{\mathrm{eq}}$ plane. By using the F-R equation (38) and Equation (3b), we find that the nonlinear resonance frequency ω_{nr} is given by

$$\omega_{\mathrm{nr}} = \omega_1 + \frac{\alpha_1\alpha_2^2\chi_3^2}{c^2}. \tag{39}$$

Thus, when only the first mode is excited by a primary resonance excitation, the plate resonates nonlinearly at the frequency $\omega_{\rm nr}$ with a first-order amplitude $a_{\rm nr}$, according to the solution (33) for $\eta(t)$. We also note that $a_{\rm nr}$ must be sufficiently small in order for the truncated terms of $O(a^3)$ to be neglected in $\eta(t)$.

7. Inflection point, softening/hardening, and saddle-nodes

For sufficiently small forcing χ_3, the amplitude $a_{\rm eq}$ is a single-valued function of the detuning parameter σ. The F-R curve has a "camel's hump" with a peak at the nonlinear resonance point. However, as the forcing parameter χ_3 increases, the camel's hump bends either to the left (softening) or to the right (hardening). An example of hardening-type behavior, which is discussed in the following section, is seen in Fig. 2. At a critical value $\chi_3^{\rm cr}$, the camel's hump loses its single-valuedness (one value of $a_{\rm eq}$ for one σ) and is multi-valued (three values of $a_{\rm eq}$ for one σ) for certain σ when $\chi_3 > \chi_3^{\rm cr}$. Therefore, an inflection point exists on the F-R curve when $\chi_3 = \chi_3^{\rm cr}$, being the transition value separating single- and multi-valued solutions. The inflection point can be shown to occur at

$$(\sigma,\ a_{\rm eq}) = \left(\sqrt{3}\,c\ \mathrm{sgn}(\alpha_1),\ \frac{\sqrt{2}\,c}{\sqrt[4]{3\,\alpha_1^2}}\right), \tag{40}$$

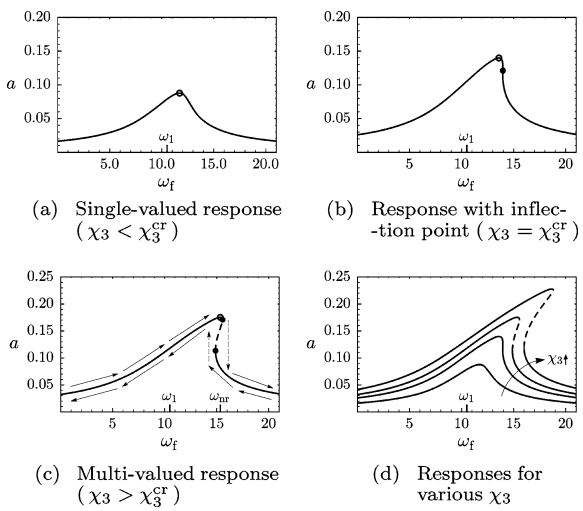

Fig. 2 F-R curves for $\beta = 100$, $\nu = 0.1$, $\tau = 1$, $\chi_0^2 = 0.5$, $F(r,t) = 0$, $c = 2$ and (a) $\chi_3 = 5$, (b) $\chi_3 = \chi_3^{\rm cr} = 7.98$, (c) $\chi_3 = 10$, or (d) multiple values of χ_3

where $\mathrm{sgn}(x)$ gives the sign of a real nonzero number x, and the critical value of χ_3 is

$$\chi_3^{\rm cr} = \left(\frac{8\,c^3}{3\sqrt{3}\,|\alpha_1|\,\alpha_2^2}\right)^{1/2}. \tag{41}$$

Then, it follows from the F-R equation and the inflection point (40) that the F-R curve bends to the left (softening) or to the right (hardening) according to the following rules:

$$\alpha_1 < 0 \implies \text{softening} \tag{42a}$$

and

$$\alpha_1 > 0 \implies \text{hardening}. \tag{42b}$$

8. Numerical results

By using the frequency-response equation (38), we can plot the equilibrium vibration amplitude $a_{\rm eq}$ (a, for short) versus the forcing frequency $\omega_{\rm f}$; that is, we can create F-R curves for general system parameters. The nonlinear resonance frequency $\omega_{\rm nr}$ is given by Equation (39) and the nonlinear resonance amplitude $a_{\rm nr}$ is the largest solution of Equation (38) for the detuning parameter from Equation (39). For computational efficiency, three modes are used to generate the curves presented in this section, and the convergence of similar curves in investigated in the next section. Furthermore, the softening or hardening nature of the nonlinearity is determined according to conditions (42), and the critical AC voltage $\chi_3^{\rm cr}$ for the onset of multi-valuedness is given by Equation (41).

In Fig. 2, we show representative frequency-response curves. For any system, a critical AC voltage $\chi_3^{\rm cr}$ exists, such that the F-R curve is single-valued for $\chi_3 < \chi_3^{\rm cr}$, as in Fig. 2(a). The solution is purely stable, being represented by a solid curve, and the nonlinear resonance point is represented by a circle. At the critical value $\chi_3^{\rm cr}$, the single-valuedness is about to break down, as in Fig. 2(b). An inflection point exists, denoted by the dot. For $\chi_3 > \chi_3^{\rm cr}$, the curve is partially multi-valued, as seen in Fig. 2(c). Two saddle-node bifurcations, also denoted by dots, now exist and the curve between them is unstable (dashed). Accordingly, hysteresis exists associated with jumps at the saddle-node bifurcations as the forcing frequency $\omega_{\rm f}$ is slowly varied up and down.

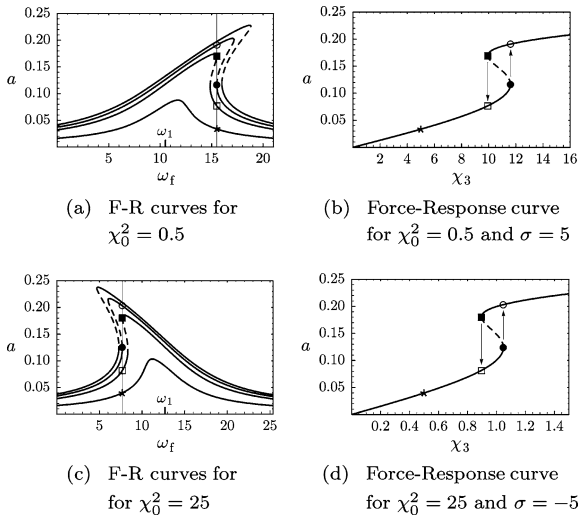

(a) F-R curves for $\chi_0^2 = 0.5$ (b) Force-Response curve for $\chi_0^2 = 0.5$ and $\sigma = 5$

(c) F-R curves for $\chi_0^2 = 25$ (d) Force-Response curve for $\chi_0^2 = 25$ and $\sigma = -5$

Fig. 3 Frequency-response and force-response curves for the system with $\beta = 100$, $\nu = 0.1$, $\tau = 1$, $F(r,t) = 0$, $c = 2$, and either (a)-(b) $\chi_0^2 = 0.5$ or (c)-(d) $\chi_0^2 = 25$

The evolution of the vibration amplitude with increasing χ_3 can be seen in Fig. 2(d). As the AC forcing χ_3 increases, a increases and the F-R curve bends to the right (hardening). Eventually, the F-R curve becomes multi-valued and hysteresis exists. We note that according to conditions (42), the nonlinearity is of the hardening type because $\alpha_1 = 157.5 > 0$.

Jumps can also be seen in force-response curves, which depict how the vibration amplitude a changes with the AC forcing χ_3 for a fixed forcing frequency ω_f, or alternatively a fixed detuning parameter σ. Example force-response curves are seen in Figs. 3(b) and (d) corresponding to the frequencies marked in Figs. 3(a) and (c), respectively. Jumps (depicted as arrows) occur in Fig. 3(b) because σ is greater than the critical value for the inflection point (40) of the hardening-type system, and amplitude jumps occur in Fig. 3(d) because σ is less than the critical inflection value of the softening-type system. Conversely, if the chosen forcing frequency ω_f does not deviate far enough from the natural frequency ω_1 for either system parameters, then no jumps in the vibration amplitude will occur.

We note that the softening/hardening nature of the plate is independent of χ_3, but is strongly dependent on the DC component χ_0, which affects equilibrium. In fact, the nature of the nonlinearity transitions from hardening to softening as χ_0 increases and the plate deflects more towards the fixed electrode. This transition is seen in the bold curve of Fig. 4. The curve

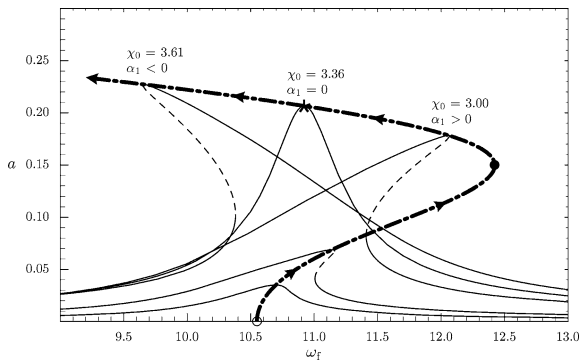

Fig. 4 Progression from hardening to softening as χ_0 increases for $\beta = 100$, $\nu = 0.1$, $\tau = 1$, $F(r,t) = 0$, $c = 0.25$, and $\chi_3 = 0.25$

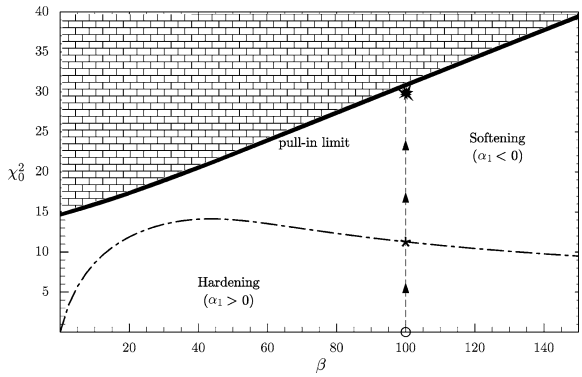

Fig. 5 Hardening and softening regions for $\nu = 0.1$, $\tau = 1$, and $F(r,t) = 0$

tracks the nonlinear resonance frequency from its position for zero χ_0 (denoted with a circle) up to pull-in (not seen in the figure). Initially, we only have a hardening-type behavior ($\alpha_1 > 0$). However, as we increase χ_0 to 3.36 (denoted by an asterisk), we find that there is neither hardening nor softening, since $\alpha_1 = 0$. Hence, the system is locally linear and the F-R curve is not bent for that case. As we increase χ_0 beyond 3.36, we find that the nonlinearity of the system becomes softening ($\alpha_1 < 0$), with the F-R curve being bent to the left, like that for $\chi_0 = 3.61$. Softening remains until the plate reaches pull-in.

The DC voltage χ_0 at the transition point ($\alpha_1 = 0$) from a hardening-type to a softening-type behavior depends on the parameters β, ν, and τ. The dependence on β for $\nu = 0.1$ and $\tau = 1$ is shown in Fig. 5. For example, when $\beta = 100$, the system being studied is that of Fig. 4. The effective nonlinearity moves from the hardening region to the softening region as χ_0 is increased. Eventually, the plate is pulled into the "brick wall" (the

fixed electrode). In fact, $\alpha_1 \to -\infty$ and $\alpha_2 \to \infty$ as the pull-in limit is approached, which means that the nonlinear resonance amplitude and frequency become increasingly sensitive to χ_3. Consequently, χ_3 must approach zero to maintain finite responses as the plate approaches pull-in.

9. Numerical convergence

We have found that stable deflections converge sufficiently with five axisymmetric modes [20]. However, in order for the reduced-order model to be of any use, the equilibrium amplitude a also has to converge as the number N of modes increases. This means that the system parameters α_1 and α_2 in the F-R equation (38) and the first undamped natural frequency ω_1 must all be sufficiently close to their limits for some N, such that the F-R curve is sufficiently converged.

We calculated α_1, α_2, and ω_1 as functions of χ_0 for various combinations of system parameters β, ν, and τ with different values of N. Because the reduced-order model is intended for analysis of CMUTs, we choose (nondimensional) system parameters feasible for typical CMUTs. We focus on modeling air transducers by restricting the nondimensional residual stress τ to be less than the nondimensional parameter β, where β is as high as 100. For simplicity, we also let Poisson's ratio ν equal 0.2 and let $F(r, t) = 0$ (no pressure difference across the plate).

Results for a combination of parameters are shown in Fig. 6. As pull-in is approached, the respective curves in Figs. 6(a)–(c) generally deviate from each other. However, three modes seem to be sufficient to characterize the dynamic-related quantities α_1, α_2, and ω_1 for most of the range of χ_0 up to pull-in. In fact, the curves for three and four modes are hardly distinguishable. At $\chi_0^2 = 13$, which is about 87% of the critical value for pull-in, the frequency-response curves in Fig. 6(d) are basically converged for three modes.

Three modes may not be sufficient for convergence, as seen in Fig. 7, where at least four modes are needed to sufficiently characterize the steady-state dynamics for most of the range up to pull-in. The curves for four and fives modes are barely distinguishable, and at $\chi_0^2 = 28$, which is about 84% of the critical value for pull-in, the F-R curves in Fig. 7(d) are basically converged for four modes.

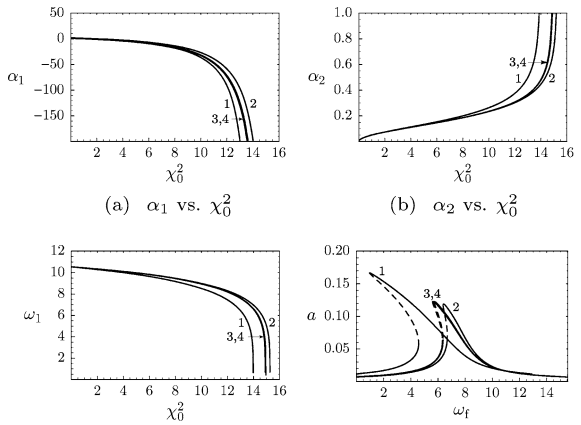

Fig. 6 Parameter and response curves for $\beta = 1, \nu = 0.2, \tau = 1$, and $F(r, t) = 0$ with different numbers of modes

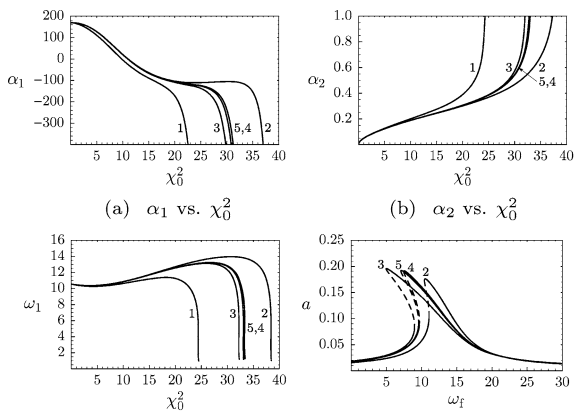

Fig. 7 Parameter and response curves for $\beta = 100$, $\nu = 0.2$, $\tau = 1$, and $F(r, t) = 0$ with different numbers of modes

The previous analysis was for systems with zero pressure difference across the plate, but advantageous pressure differences exist in many CMUTs. For instance, when a vacuum is created under the plate and the pressure from a fluid acts on its top, the electromechanical coupling increases due to the plate deflection, making the system more efficient for conversion of electrical energy to mechanical energy [8]. We would like the macromodel to be applicable for such situations. In this spirit, we let $F(r, t)$ be constant and test convergence for feasible cases, one of which is seen in Fig. 8. For all four values of F, four modes are sufficient for convergence for most of the range up to the respective pull-in. However, as F increases, the curves deviate

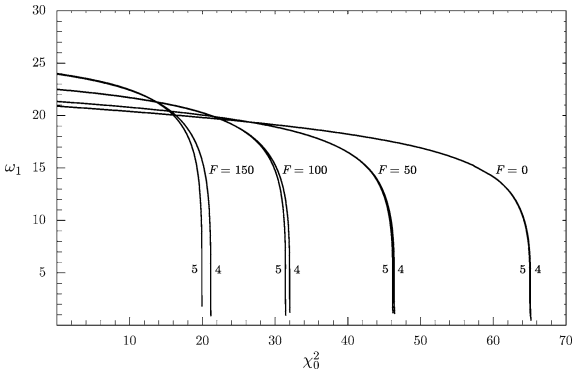

Fig. 8 First undamped natural frequency for $\beta = 50$, $\nu = 0.2$, $\tau = 50$, and (for paired curves from left to right) $F(r,t) = 150$, $F(r,t) = 100$, $F(r,t) = 50$, or $F(r,t) = 0$ for four or five modes

more and five modes become necessary for convergence.

In general, at least three ($N = 3$) modes should be used in the reduced-order model (2) to characterize the responses of clamped circular plates used in air-immersed CMUTs to primary resonance excitations. In fact, three modes were used to generate the curves in Figs. 2–5. Consequently, the error in the approximate equilibrium solution (33) is mainly due to truncation at a certain order of a in the method of multiple scales and not due to the truncation of the number N of modes in the reduced-order model. In practice, however, the nondimensional amplitude a will be sufficiently small, such that the number N of modes primarily limits the accuracy of the approximate amplitudes.

10. Conclusions

We used an analytical reduced-order model (macromodel) to investigate the response of an electrostatically actuated clamped circular plate to a primary resonance excitation of its first axisymmetric mode. The method of multiple scales was used to derive a semi-analytical expression for the equilibrium amplitude of vibration. The plate was found to always transition from a hardening-type to a softening-type behavior as the DC voltage increases towards pull-in.

We found that, in general, at least three linear undamped axisymmetric modes are needed to characterize the equilibrium amplitude of vibration for primary resonance excitation of clamped circular plates used in many capacitive micromachined ultrasonic transducers. Sufficient convergence up to pull-in seems to be met for feasible CMUTs if five modes are used, but one should inspect the frequency-response curves for assurance of convergence.

Our macromodel can be used as an effective design tool for CMUTs for multiple reasons. First, the equilibrium-amplitude expressions allow for general residual stress and material and geometric design variables. For instance, the nonlinear resonance point of any system can easily be calculated for multiple values of the AC voltage forcing. Second, our model eliminates the computational problems near pull-in found in many FEM-based models, because the amplitudes near pull-in can be calculated as fast as those away from the instability. Third, our model allows for bending-dominated plates, which is desirable for CMUTs in which the residual stress is negligible. Fourth, the reduced-order model presented here accounts for the first geometric nonlinearity of the von Kármán type. Consequently, any increase in frequency due to strain hardening is accounted for, as seen in Fig. 7(c) in which the frequency can increase instead of always decrease with deflection as in Fig. 6(c).

Appendix A: Matrix and vector definitions for reduced-order model

In this appendix, we reduce the reduced-order model developed in a previous paper [21] to the matrix form in Equation (2). First, we let

$$\psi'_{mn}(r) = \varphi_{1mn}(r) + \frac{1+\nu}{1-\nu}\varphi_{2mn}(r), \tag{43}$$

where

$$\varphi_{1mn}(r) = \frac{1}{4r}\int_0^r \xi\phi'_m\phi'_n d\xi + \frac{r}{4}\int_r^1 \frac{\phi'_m\phi'_n}{\xi} d\xi \tag{44a}$$

and

$$\varphi_{2mn}(r) = \frac{r}{4}\int_0^1 \xi\phi'_m\phi'_n d\xi. \tag{44b}$$

The reduced-order model then becomes

$$\begin{aligned}
&\left(\ddot{\eta}_q + 2c\dot{\eta}_q + \Omega_q^2\eta_q\right) - 2\left(\ddot{\eta}_m + 2c\dot{\eta}_m + \Omega_m^2\eta_m\right)\eta_i A_{imq} \\
&\quad + \left(\ddot{\eta}_m + 2c\dot{\eta}_m + \Omega_m^2\eta_m\right)\eta_i\eta_j B_{ijmq} \\
&= \beta\left[-\eta_m\eta_n\eta_p\left(C_{1mnpq} + \frac{1+\nu}{1-\nu}C_{2mnpq}\right)\right. \\
&\quad + 2\eta_i\eta_m\eta_n\eta_p\left(D_{1imnpq} + \frac{1+\nu}{1-\nu}D_{2imnpq}\right) \\
&\quad \left. -\eta_i\eta_j\eta_m\eta_n\eta_p\left(E_{1ijmnpq} + \frac{1+\nu}{1-\nu}E_{2ijmnpq}\right)\right] \\
&\quad -\tau\eta_m F_{mq} + 2\tau\eta_i\eta_m G_{imq} - \tau\eta_i\eta_j\eta_m H_{ijmq} \\
&\quad + I_q - 2\eta_i J_{iq} + \eta_i\eta_j K_{ijq} + v^2(t)L_q, \qquad (45)
\end{aligned}$$

where

$$A_{imq} = \int_0^1 r\phi_i\phi_m\phi_q dr, \qquad (46a)$$

$$B_{ijmq} = \int_0^1 r\phi_i\phi_j\phi_m\phi_q dr, \qquad (46b)$$

$$C_{1mnpq} = \int_0^1 \phi_q'\phi_m'\varphi_{1np} dr, \qquad (46c)$$

$$C_{2mnpq} = \int_0^1 \phi_q'\phi_m'\varphi_{2np} dr, \qquad (46d)$$

$$D_{1imnpq} = \int_0^1 (\phi_i\phi_q)'\phi_m'\varphi_{1np} dr, \qquad (46e)$$

$$D_{2imnpq} = \int_0^1 (\phi_i\phi_q)'\phi_m'\varphi_{2np} dr, \qquad (46f)$$

$$E_{1ijmnpq} = \int_0^1 (\phi_i\phi_j\phi_q)'\phi_m'\varphi_{1np} dr, \qquad (46g)$$

$$E_{2ijmnpq} = \int_0^1 (\phi_i\phi_j\phi_q)'\phi_m'\varphi_{2np} dr, \qquad (46h)$$

$$F_{mq} = \int_0^1 r\phi_m'\phi_q' dr, \qquad (46i)$$

$$G_{imq} = \int_0^1 r\phi_m'(\phi_i\phi_q)' dr, \qquad (46j)$$

$$H_{ijmq} = \int_0^1 r\phi_m'(\phi_i\phi_j\phi_q)' dr, \qquad (46k)$$

$$I_q = \int_0^1 Fr\phi_q dr, \quad J_{iq} = \int_0^1 Fr\phi_i\phi_q dr, \qquad (46l)$$

$$K_{ijq} = \int_0^1 Fr\phi_i\phi_j\phi_q dr, \quad L_q = \int_0^1 r\phi_q dr, \qquad (46m)$$

for $q = 1, 2, \ldots, N$, and the summation signs have been removed in Equation (45) for notation simplification. Therefore, all terms in Equation (45) are created by summing over their respective lower-case Latin indices (excluding q), which range from 1 to N.

Because all integrands in Equations (46) are known explictly after a function $F(r, t)$ is chosen, the integrals can be evaluated numerically one time and saved for use in Equation (45). Thus, the variables with upper-case Latin names in Equation (45) are simply known constants.

Finally, we simplify the form of Equation (45) by putting the N coupled equations ($q = 1, 2, \ldots, N$) into matrix form. We collect all $\eta_i(t)$ into a column vector $\boldsymbol{\eta}(t)$; that is,

$$\boldsymbol{\eta}(t) = \{\eta_1(t),\ \eta_2(t), \ldots,\ \eta_N(t)\}, \qquad (47)$$

and then rearrange Equation (45) to obtain Equation (2); that is,

$$M(\boldsymbol{\eta})\ddot{\boldsymbol{\eta}} + 2cM(\boldsymbol{\eta})\dot{\boldsymbol{\eta}} + N(\boldsymbol{\eta})\boldsymbol{\eta} = \boldsymbol{P}(\boldsymbol{\eta}) + v^2(t)\boldsymbol{L},$$

where

$$M(\boldsymbol{\eta}) = [M_{qs}(\boldsymbol{\eta})] = [\delta_{qs} - 2\eta_i A_{isq} + \eta_i\eta_j B_{ijsq}], \qquad (48a)$$

$$\begin{aligned}
N(\boldsymbol{\eta}) &= [N_{qs}(\boldsymbol{\eta})] \\
&= \left[\Omega_q^2\delta_{qs} - 2\Omega_s^2\eta_i A_{isq} + \Omega_s^2\eta_i\eta_j B_{ijsq}\right], \qquad (48b)
\end{aligned}$$

$$\begin{aligned}
\boldsymbol{P}(\boldsymbol{\eta}) &= \{P_q(\boldsymbol{\eta})\} \\
&= \left\{\beta\left[-\eta_m\eta_n\eta_p\left(C_{1mnpq} + \frac{1+\nu}{1-\nu}C_{2mnpq}\right)\right.\right. \\
&\quad + 2\eta_i\eta_m\eta_n\eta_p\left(D_{1imnpq} + \frac{1+\nu}{1-\nu}D_{2imnpq}\right) \\
&\quad \left.\left. -\eta_i\eta_j\eta_m\eta_n\eta_p\left(E_{1ijmnpq} + \frac{1+\nu}{1-\nu}E_{2ijmnpq}\right)\right]\right. \\
&\quad -\tau\eta_m F_{mq} + 2\tau\eta_i\eta_m G_{imq} - \tau\eta_i\eta_j\eta_m H_{ijmq}
\end{aligned}$$

$$+I_q - 2\eta_i J_{iq} + \eta_i \eta_j K_{ijq} \Big\}, \tag{48c}$$

$\boldsymbol{L} = \{L_q\}$, δ_{qs} is the Kronecker delta, and the summation signs have been removed in Equations (48) for notation simplification.

References

1. Haller, M.I., Khuri-Yakub, B.T.: A surface micromachined electrostatic ultrasonic air transducer. In: Proc. of IEEE Ultrasonics Symp. Cannes, France, Vol. 2, pp. 1241–1244 (1994)
2. Ladabaum, I., Khuri-Yakub, B.T., Spoliansky, D., Haller, M.I.: Micromachined ultrasonic tranducers (MUTs). In: Proc. of IEEE Ultrasonics Symp., Seattle, WA, Vol. 1, pp. 501–504 (1995)
3. Haller, M.I., Khuri-Yakub, B.T.: A surface micromachined electrostatic ultrasonic air transducer. IEEE Trans. Ultrason., Ferroelectr. Freq. Control **43**, 1–6 (1996)
4. Jin, X., Ladabaum, I., Khuri-Yakub, B.T.: The microfabrication of capacitive ultrasonic transducers. J. Microelectromech. Syst. **7**, 295–302 (1998)
5. Hansen, S.T., Turo, A., Degertekin, F.L., Khuri-Yakub, B.T.: Characterization of capacitive micromachined ultrasonic transducers in air using optical measurements. In: Proc. of IEEE Ultrasonics Symp., San Juan, Puerto Rico, Vol. 1, pp. 947–950 (2000)
6. Yaralioglu, G.G., Ergun, A.S., Bayram, B., Marentis, T., Khuri-Yakub, B.T.: Residual stress and young's modulus measurement of capacitive micromachined ultrasonic transducer membranes. In: Proc. of IEEE Ultrasonics Symp., Atlanta, GA, Vol. 2, pp. 953–956 (2001)
7. Caronti, A., Majjad, H., Ballandras, S., Caliano, G., Carotenuto, R., Iula, A., Foglietti, V., Pappalardo, M.: Vibration maps of capacitive micromachined ultrasonic transducers by laser interferometry. IEEE Trans. Ultrason., Ferroelectr. Freq. Control **49**, 289–292 (2002)
8. Huang, Y., Ergun, A.S., Hæggström, E., Badi, M.H., Khuri-Yakub, B.T.: Fabricating capacitive micromachined ultrasonic transducers with wafer-bonding technology. J. Microelectromech. Syst. **12**, 128–137 (2003)
9. Yaralioglu, G.G., Ergun, A.S., Bayram, B., Hæggström, E., Khuri-Yakub, B.T.: Calculation and measurement of electromechanical coupling coefficient of capacitive micromachined ultrasonic transducers. IEEE Trans. Ultrason., Ferroelectr. Freq. Control **50**, 449–456 (2003)
10. Ladabaum, I., Jin, X., Soh, H.T., Pierre, F., Atalar, A., Khuri-Yakub, B.T.: Microfabricated ultrasonic transducers: towards robust models and immersion devices. In: Proc. of IEEE Ultrasonics Symp., San Antonio, TX, Vol. 1, pp. 335–338 (1996)
11. Jin, X., Oralkan, Ö., Degertekin, F.L., Khuri-Yakub, B.T.: Characterization of one-dimensional capacitive micromachined ultrasonic immersion transducer arrays. IEEE Trans. Ultrason. Ferroelectr. Freq. Control **48**, 750–760 (2001)
12. Ergun, A.S., Cheng, C-H., Demirci, U., Khuri-Yakub, B.T.: Fabrication and characterization of 1-dimensional and 2-dimensional capacitive Micromachined ultrasonic transducer (CMUT) arrays for 2-dimensional and volumetric ultrasonic imaging. In: Proc. of Oceans '02 MTS/IEEE, Biloxi, MS, Vol. 4, pp. 2361–2367 (2002)
13. Bozkurt, A., Degertekin, F.L., Atalar, A., Khuri-Yakub, B.T.: Analytic modeling of loss and cross-coupling in capacitive micromachined ultrasonic transducers. In: Proc. of IEEE Ultrasonics Symp., Sendai, Japan, Vol. 2, pp. 1025–1028 (1998)
14. Bozkurt, A., Ladabaum, I., Atalar, A., Khuri-Yakub, B.T.: Theory and analysis of electrode size optimization for capacitive microfabricated ultrasonic transducers. IEEE Trans. Ultrason. Ferroelectr. Freq. Control. **46**, 1364–1374 (1999)
15. Bayram, B., Yaralioglu, G.G., Ergun, A.S., Khuri-Yakub, B.T.: Influence of the electrode size and location on the performance of a CMUT. In: Proc. of IEEE Ultrasonics Symp., Atlanta, GA, Vol. 2, pp. 949–952 (2001)
16. Buhrdorf, A., Ahrens, O., Binder, J.: Capacitive micromachined ultrasonic transducers and their application. In: Proc. of IEEE Ultrasonics Symp., Atlanta, GA, Vol. 2, pp. 933–940 (2001)
17. Pelesko, J.A., Chen, X.Y.: Electrostatic deflections of circular elastic membranes. J. Electrost. **57**, 1–12 (2003)
18. Yu, M., Balachandran, B.: Sensor diaphragm under initial tension: linear analysis. Exp. Mech. **45**, 123–129 (2005)
19. Li, G., Aluru, N.R.: Linear, nonlinear, and mixed-regime analysis of electrostatic MEMS. Sensors Actuators A **91**, 278–291 (2001)
20. Vogl, G.W., Nayfeh, A.H.: A reduced-order model for electrically actuated clamped circular plates. In: Proc. of ASME Design Engineering Technical Conf., Chicago, IL, DETC VIB-48530 (2003)
21. Vogl, G.W., Nayfeh, A.H.: A reduced-order model for electrically actuated clamped circular plates. J. Micromech. Microeng. **15**, 684–690 (2005)
22. Nayfeh, A.H.: Perturbation Methods, Wiley, New York, pp. 228–236 (1973)
23. Nayfeh, A.H.: Introduction to Perturbation Techniques, Wiley, New York, pp. 122–127 (1981)
24. Nayfeh, A.H., Mook, D.T.: Nonlinear Oscillations, Wiley, New York, pp. 366–367 (1979)
25. Nayfeh, A.H.: Nonlinear Interactions: Analytical, Computational, and Experimental Methods, Wiley, New York, p. xvi (2000)